

# Speed and location tracking of moving multiphase interfaces via a capacitance microsensor array during droplet evaporation

Md Tanbir Hasan Mondal<sup>a</sup>, Rifat-E-Nur Hossain<sup>a</sup>, Ronald Martin<sup>b</sup>, Arden L. Moore<sup>a,c,\*</sup>

<sup>a</sup> Institute for Micromanufacturing, Louisiana Tech University, Ruston, LA 71272, USA

<sup>b</sup> Electrical Engineering Dept., Louisiana Tech University, Ruston, LA 71272, USA

<sup>c</sup> Mechanical Engineering Dept., Louisiana Tech University, Ruston, LA 71272, USA



## ARTICLE INFO

**Keywords:**  
Moving contact lines  
Phase change  
Evaporation  
Droplet detection  
Capacitance sensing

## ABSTRACT

Knowledge of the location and speed of a moving multiphase contact line provides significant and valuable insights into the fundamental physics behind condensation- and evaporation-based processes such as occur in high heat flux thermal management solutions. From an application perspective, this information can be leveraged to ascertain and enhance device design and performance of phase change-based cooling processes. In this work, we present a capacitance-based phase interface sensing approach capable of measuring the location and speed of a moving multiphase interface at the microscale, evaluate the impact of substrate material on its performance, and demonstrate its ability to function at elevated temperatures during water droplet evaporation. The sensing is accomplished via an array of planar interdigitated electrodes upon either a doped semiconductor or dielectric substrate. Measuring capacitance changes with time facilitates sensing of the contact line as it passes over each electrode pair. This capacitive sensing scheme is noninvasive to the system under study, allowing its implementation into many types of existing hardware and devices and does not require optical access to the phase change area of the device. Results for unconstrained water droplets are presented, and it is shown that the choice of substrate material has a marked impact on sensing behavior in terms of sensor coupling. Finally, data for the moving multiphase contact line of an evaporating water droplet is presented to demonstrate functionality at elevated temperatures and during a dynamic heat transfer process.

## 1. Introduction

In a given three-phase system such as for a growing vapor bubble or condensing/evaporating droplet, the three-phase contact line occurs at the interface of the liquid, solid, and gas phases. This three-phase contact line is able to move along the surface of the solid as the individual bubble or droplet expands or contracts. Moving contact line (MCL) has been a subject of extensive experimental and analytical studies because of its ubiquity in interfacial science and many engineering fields, including but not limited to microfluidic devices, various coating and printing technologies, phase-change heat transfer systems, two-phase flows in porous media, and nucleate boiling [1–5]. The strong temperature and density gradients in the vicinity of MCL along with its mobile nature make it a major factor in determining the overall heat transfer characteristics of the phase change process. As a result, the MCL behavior has also been investigated in recent years as it is the region that facilitates the highest heat transfer in evaporative or other

phase-change heat transfer processes [6–10]. In terms of thermal management applications, the widespread utilization of multiphase cooling strategies to handle high heat flux densities means that insights gained into the behavior of the MCL and its associated thermal impacts can lead to improved cooling devices, processes, and effectiveness via informed surface engineering. Studying MCL behavior for phase-change heat transfer processes like droplet evaporation has also become significant as temperature data alone does not provide a comprehensive understanding. It requires revealing the interdependence of MCL speed and location with heat transfer mechanisms involved in phase-change heat transfer processes [9,11–13].

Although optical sensing has been the most prevalent technique with in the literature to study an MCL in laboratory settings, electrical sensing schemes have advantages over optical techniques in terms of precision, stability, and applicability at the microscale [14,15] or in situations where visual access is blocked such as within heat exchangers, vapor chambers, or other opaque enclosures. Optical techniques possess

\* Corresponding author at: Institute for Micromanufacturing, Louisiana Tech University, Ruston, LA 71272, USA.  
E-mail address: [amoore@latech.edu](mailto:amoore@latech.edu) (A.L. Moore).

flow sensitivity and throughput, often require bulky and complex setups, and are unsuitable for close-packed integration. On the other hand, electrical detection comprising resistive and capacitive sensing facilitate high sensitivity, scalability, transient response, flow cost, and compatibility in compact integration [16–18]. Resistive and capacitive sensing have been most prominent in electrical techniques, with some important differentiators between the two types. Resistive sensing has some known limitations involving a continuous conductive phase in the sensing region and intricate patterns to achieve effective performance [14]. In contrast, capacitive sensing requires only a spatial separation between two coplanar electrodes for achieving sensing and can be more easily scaled down to smaller feature sizes due to its less complicated geometry requirements [19].

In this work, we present a capacitance-based microdevice capable of tracking the spatial location and motion of the moving MCL, evaluate the impact of substrate material on its performance, and demonstrate its ability to function at elevated temperatures during water droplet evaporation. As shown in Fig. 1, the microdevice is comprised of a total of six capacitive micro-sensors based on coplanar interdigitated electrodes (IDEs) with a thin insulating polymer layer on top. This approach also facilitates a bulk micro-fabrication compatible means of sensing phase interface such that many sensors can be created at one time. Unlike existing optical methods used previously in literature [10,20,21], this micro-sensor array approach does not require visual access to the surface under study such that MCL tracking can occur within opaque hardware or enclosures. Our previous work on tracking MCL location via this type of sensing scheme on a semiconducting substrate was shown to be effective for simple aspirated water droplets but also demonstrated certain nonidealities, particularly in terms of capacitive coupling effects between sensors in close proximity [22]. Here, we report on significant improvements by utilizing a dielectric substrate, including but not limited to obtaining a much stronger capacitance signal output from multiple sensors in adjacent proximity with reduced coupling effects. The motivations behind choosing soda-lime glass as the alternate substrate are its cost-effectiveness and broad applicability in microfluidic and other MEMS devices. Soda-lime glass substrates are also widely implemented as they provide advantages over other materials in terms of high electrical insulation, surface stability, high resistance to mechanical stress, and compatibility with a wide range of microfabrication

techniques [23–25]. We also report for the first-time data for the moving MCL of an evaporating water droplet to demonstrate this approach's functionality at elevated temperatures and during a dynamic and realistic heat transfer process.

## 2. Methodology

### 2.1. Operating principle

The basic operating principle of this phase interface sensing microdevice is based on changes in the relative permittivity of the medium directly above the interdigitated electrodes with the passage of the MCL, which in turn causes a change in capacitance signals obtained from the sensor array [14,15,22]. Apart from the relative permittivity of the medium  $\epsilon_{r, \text{eff}}$ , the capacitance  $C$  of the sensor array depends on the width  $w$  and spacing  $2a$  between two consecutive coplanar electrodes. The following equation can be employed to calculate the capacitance  $C$  in the sensor array [26],

$$C = \frac{2\epsilon_{r, \text{eff}}\epsilon_0 l}{\pi} \left[ \frac{1}{1 + \frac{w}{a}} + \frac{\pi}{1 + \frac{w}{a}} - 1 \right] \quad (1)$$

where,  $\epsilon_0$  is the vacuum permittivity and  $l$  is the interaction length of the electrode pair. Fig. 1(a) demonstrates a schematic illustration of the capacitive sensing scheme, where electric field lines between two planar electrodes extend above the thin insulating layer to interact with the motion of MCL as the liquid droplet passes over it. These electric field lines are caused by an applied sensing voltage to the electrode pair. The sensing range of the electrical field from the top surface of the IDEs (referred to as the penetration depth  $T$ ) also varies with the width  $w$  and spacing  $2a$  between two consecutive coplanar electrodes by following the equation below [26].

$$T = \text{asinh} \left[ \cosh^{-1} \left( \frac{1 + \frac{w}{a}}{a} \right) \right] = a \left[ \frac{\pi}{1 + \frac{w}{a}} - 1 \right] \quad (2)$$

### 2.2. Microdevice overview

The microdevice design in this work contains six capacitive sensors

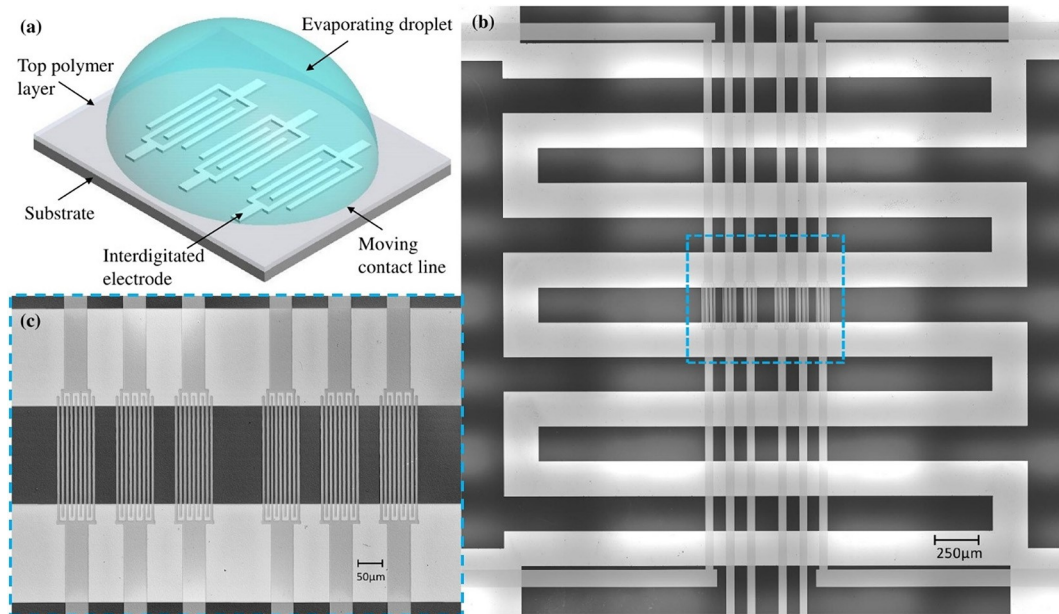


**Fig. 1.** (a) A conceptual illustration of the capacitive sensing scheme (not to scale). (b) A fluorescence image of the microdevice showing resistance heater and capacitance micro-sensor array. (c) A detailed view of the sensing zone enclosed by the dashed box in (b) showing six capacitive sensors based on interdigitated electrodes. The resistance heater and interdigitated electrodes are on separate device layers and separated by a polymer thin film as described in the main text.

as shown in Fig. 1, with each sensor being comprised of an IDE pair. The sensitivity or strength of the capacitance signal and penetration depth of the electric field lines depends on the geometry of the IDEs. The measured capacitance and penetration depth increase with the increasing width of the electrodes. However, the capacitance decreases with increasing spacing between electrodes. The strength of the capacitive signal also increases with the number of electrodes and their interaction length [27]. Although increasing width, interaction length, and the number of electrodes would enhance the sensitivity of the sensing scheme, it would also reduce the spatial sensitivity of the microdevice because of its increasing physical dimensions. Narrower spatial separation between two consecutive electrodes will also lead more challenging microfabrication and a reduction in the number of defect-free devices. Hence, a balanced approach has been implemented during the device design to facilitate a workable compromise between magnitude of the capacitive signal, penetration depth, desired spatial resolution, and high yield microfabrication. The final IDE array design shown in Fig. 1(b-c) has an electrode width of  $w = 6\mu\text{m}$ , spacing between two consecutive electrodes  $a = 3\mu\text{m}$ , and an interaction length of  $l = 250\mu\text{m}$ .

### 2.3. Micro-fabrication process

Identical capacitance-sensing microdevice arrays were fabricated on two different substrate types in order to evaluate the impact substrate material can have on MCL sensing performance. Commercially available single side polished 500  $\mu\text{m}$  thick boron-doped ( $1 \times 10^6 \text{ cm}^{-3}$ ) silicon wafers with a 500 nm thermally grown oxide layer on top were obtained to serve as a semiconducting substrate, while soda-lime glass wafers of similar thickness were obtained to act as a dielectric substrate type. The microfabrication of the capacitive micro-sensor array consisted of photolithography, deposition of platinum (Pt), spin-coating of a thin insulating polyimide top layer, and selective etching/patterning of the deposited polymer layer by reactive-ion etching. To enable a heated surface during the droplet evaporation testing, a 100 nm thin film of Pt was deposited and patterned as a resistance heater directly on top of the starting substrate via photolithography and DC sputtering deposition. A 1.2  $\mu\text{m}$  thin film of the polyimide was deposited between the resistance heater and the IDE arrays via spin coating of the diluted polyimide (75% PI-2661 + 25% NMP) to provide an electrically insulating layer. Microdevices that were not intended for evaporation studies did not include these processing steps and instead began with the IDE microfabrication steps that follow. To create the IDE sensing array, a 70 nm thin film of Pt was deposited and patterned via DC sputtering in an AJA ATC sputtering system with a commercially available Pt target. A spin-on polymer of polyimide (PI-2611) was obtained from HD Microsystems which can be diluted with the addition of N-Methyl-2-Pyrrolidone (NMP) to achieve thinner layers. A 440 nm thin film of polyimide was deposited on top of the deposited Pt layer via spin coating of the diluted polyimide (50% PI-2661 + 50% NMP) in a closed-bowl spin coater. The 440 nm thick polyimide layer was chosen to ensure a balanced approach of increasing the sensitivity of the microdevice and providing a thick enough protective coating atop the Pt layer to prevent it from creating surface protrusions. The polyimide layer was patterned by reactive ion etching (RIE) to open contact windows at the device periphery for facilitating wire bonding between bond pads of the device and the chip carrier.

### 2.4. Signal processing

The microdevice was first soldered and wire bonded with a commercially available lead-free ceramic chip carrier, where each of the bond pads is individually connected to a pin at the backside. The microdevice and chip carrier assembly interfaces with a computer-controlled data acquisition system through a pin grid array (PGA) socket. A supporting circuit was employed to translate capacitance changes into

voltage readings and to ensure a measurable change in signal magnitude, as the capacitance changes related to this sensing scheme can be relatively small. As shown in Fig. 2(b), the supporting circuit contains an RC oscillator couple, an operational amplifier, and a reference capacitor connected in parallel with the sensing IDE capacitor. The planar interdigitated electrode arrays used for the six capacitance micro-sensor are identical in geometry and have an average capacitance of 175 fF before the experiments in the dry state with approximately 14% of sensor-to-sensor variation. Observation of the noise level indicates that the noise limit of detecting capacitance changes is 0.2 fF, which is approximately 0.11% of the average capacitance of the microsensors in the dry state. An important matter to mention here is that, from a sensing perspective, if the only goal is to determine the presence or lack of the liquid with the sensing field of a given sensor, an edge-triggered digitization scheme or signal inverter would enhance the clarity of the obtained signal compared to the technique used in the current work.

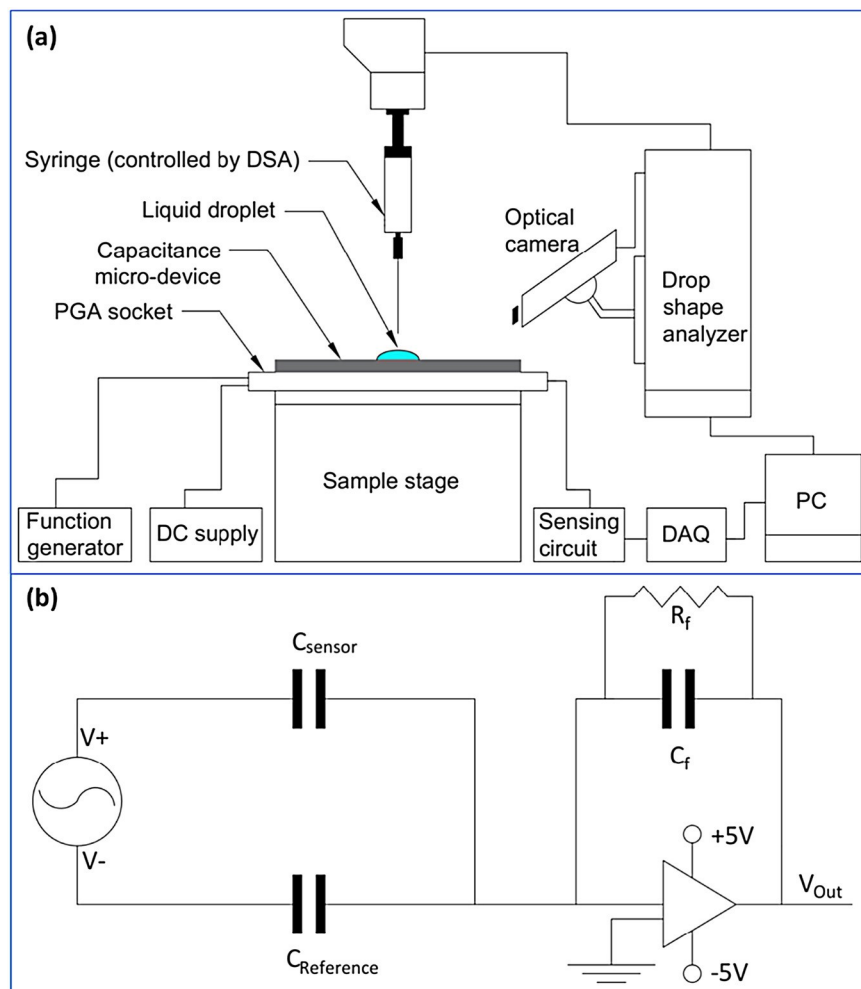
### 2.5. Experimental setup

Fig. 2(a) shows a simplified schematic of the experimental setup, where the microdevice was placed on a sample stage beneath a syringe controlled by a drop shape analyzer (DSA 25E, KRÜSS Scientific). The DSA provided controlled dosing and retraction of deionized water droplets during initial aspiration experiments that did not involve a heated substrate for droplet evaporation, and controlled deployment of a known starting droplet size for the evaporation studies that followed. An optical camera attached to the DSA also monitored the macroscopic behavior of the MCL, which served to validate that the microdevice array was functioning as intended. The captured images/videos via DSA shown in Figs. 3 and 4 also facilitated a useful comparison of the MCL speed between the microdevice and the optical technique. Simple dosing and retraction without substrate heating (i.e. aspiration) was first utilized to study the impact of substrate material on sensing behavior.

Once the dielectric substrate was found to be superior through these early studies, evaporating droplet testing at elevated device temperatures was performed. For ensuring elevated surface temperature during the droplet evaporation experiment, the thin film resistance heater of the microdevice was powered with known voltage and current from a DC power supply. Before dosing the water droplet, the resistance heater was powered by a set electric input power via the DC supply to attain the desired surface temperature of the microdevice. The DSA provided controlled dosing of the water droplet at various surface temperatures and recorded the entire evaporation process that followed. The calibration of surface temperature at various electric power inputs to the resistance heater was carried out by employing an IR camera (FLIR A300) and a commercially available thermocouple, with the latter being in good thermal contact with the center of the device. This calibration was performed after all MCL sensing activities were completed to avoid damaging the wetted surface region.

## 3. Results and discussion

The normalized capacitance changes with time were measured for a cycle of dosing and retraction of deionized water droplets for identical microdevices fabricated on either a semiconducting (doped silicon) or dielectric (soda-lime glass) substrate. Fig. 5 demonstrates the changes in capacitance signals for the capacitance micro-sensor array deposited on a silicon substrate. As Fig. 5 shows, during dosing of the water droplet, the MCL associated with the droplet's leading edge first moves over capacitance sensor CS-1 and causes an increase in signal. The MCL next reaches capacitance sensor CS-6, which also demonstrates a rise in capacitance signal with the passage of the MCL. These events are reversed when the water droplet leaves the sensing zone of the microdevice. This effectively demonstrates the basic measurement principle of measuring the capacitance changes with time as the MCL passes over the capacitance sensors. The four dashed boxes shown in Fig. 5 demonstrate



**Fig. 2.** (a) Schematic of the experimental setup for tracking speed and flocation of MCL with a capacitance-based phase interface sensing microdevice, (b) Schematic of the supporting electric circuit used for each IDE electrode pair.

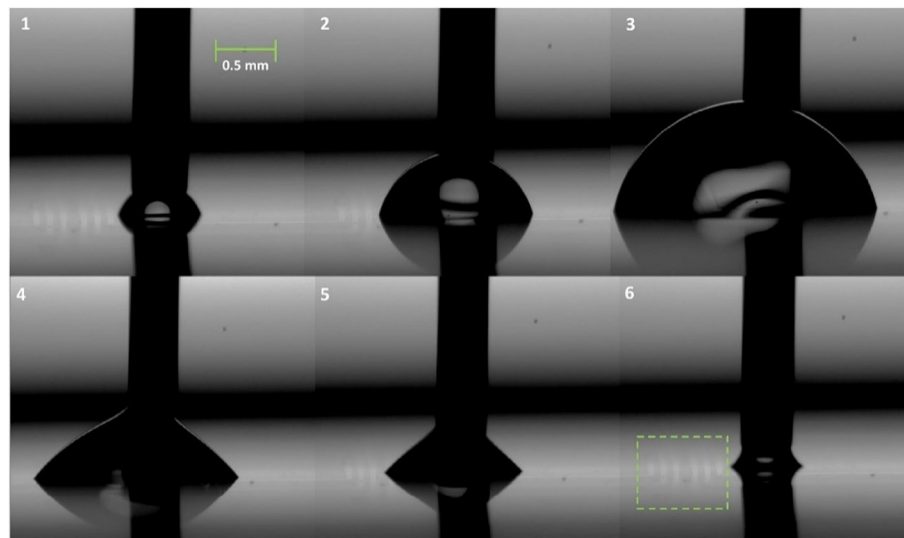


**Fig. 3.** Optical images of gradual dosing (Images 1–3) and retraction (Images 4–6) of a water droplet captured by the drop shape analyzer tool during aspiration experiments on substrate effects. The dashed box in Image 6 shows the location of the sensing zone of the microdevice comprising six capacitance sensors CS-1 to CS-6 (numbered left to right).

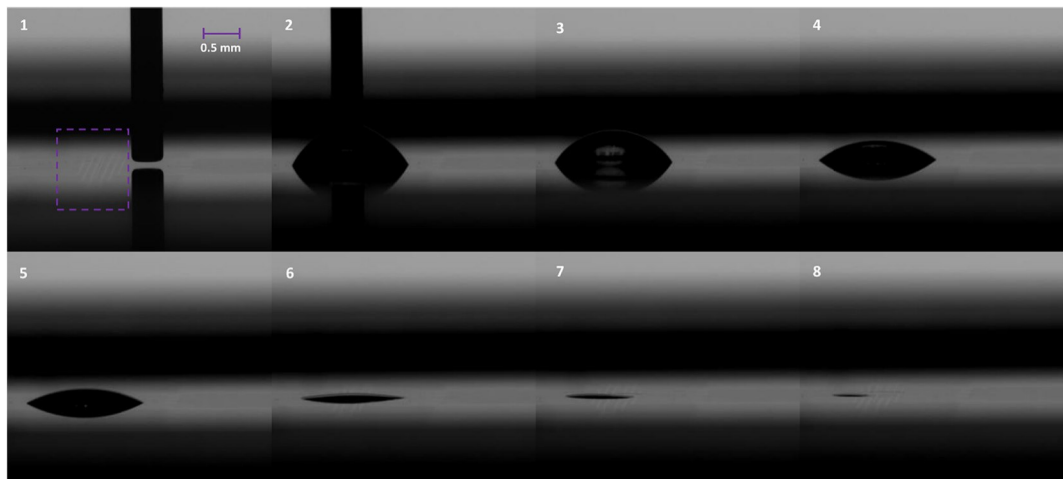


**Fig. 4.** Optical images of the evaporation process of a water droplet captured by drop shape analyzer equipment during the experiment. The dashed box in Image 1 shows the location of the sensing zone of the microdevice.

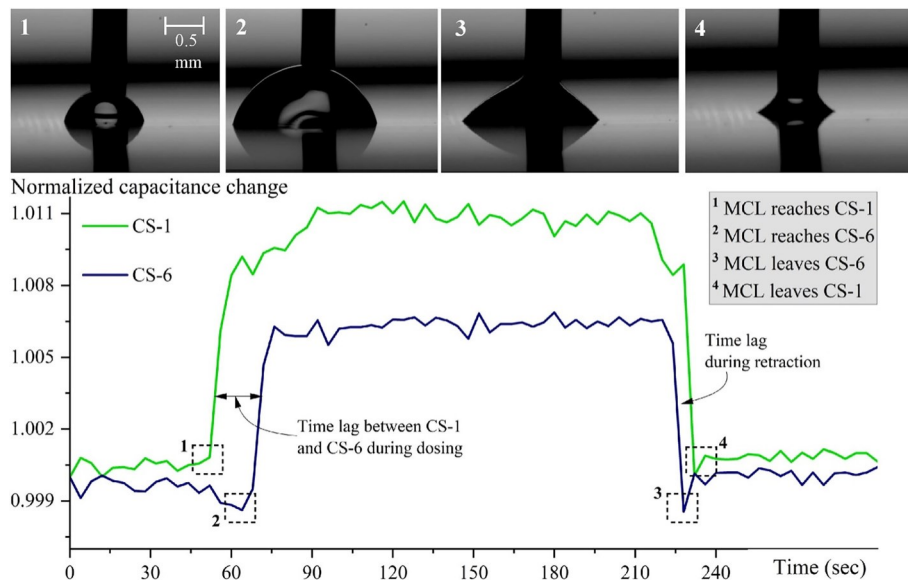


**Fig. 5.** Measured normalized capacitance changes for advancing and receding defonized water droplets using the sensor pair CS-1 and CS-6 on a doped silicon substrate, where the dashed boxes denote the significant movements of MCL as shown in the optical images on top.

the MCL's significant advancing and receding movement toward and away from the sensors employed during the experiment. The optical images on top of Fig. 5 represent MCL's corresponding fundamental movements, while the corresponding images shown in Fig. 3 exhibit the overall aspiration experiments comprising gradual dosing and retraction of water droplets. The capacitance change data presented in this work has been normalized relative to the initial capacitance signal before the experiment when only air alone was present over the sensing zone.

The captured images of gradual dosing and retraction of the water droplets shown in Fig. 3 are in good agreement with the timing of the observed capacitance changes, which helps confirm that the observed signal changes are due to passage of the droplet's MCL and no other phenomena. Besides indicating MCL location at a specific time, the measured capacitance changes also enable measurement of MCL speed by utilizing the time lag shown in the graphs and the known spatial separation between the capacitance sensors. For example, as shown in Fig. 5, during dosing the water droplet first reached CS-1 at  $t_1 = 52$  sec and the change in capacitance signal for CS-6 was detected at  $t_2 = 64$  sec. Utilizing this time lag  $\Delta t = t_2 - t_1 = 12.0$  sec and the known

distance ( $\Delta x = 658 \mu\text{m}$ ) between CS-1 and CS-6 the speed of the MCL was calculated as  $54.8 \mu\text{m/s}$  by applying  $v = \Delta x / \Delta t$ .

Despite its demonstrated functionality, the capacitance sensing with the microdevice based on doped silicon substrate exhibited some undesirable sensor proximity effects with the simultaneous implementation of three or more (out of six total) capacitance sensors to track the MCL. As an example, Fig. 6 shows the normalized capacitance changes for capacitance sensors CS-1, CS-3, and CS-6 on a doped silicon substrate, where the capacitance signal from the middle sensor is inverted from the expected trends shown in Fig. 5. This signal inversion did not cause any interruptions in the ability to track the MCL as the signal response is still present even with an inverted trend, but it represents an undesirable effect on the signal.

By repeating the same fabrication and testing procedure for sensors supported on a dielectric soda lime glass substrate, it was found that using a dielectric substrate as the device base minimized the proximity effect that caused the inversion of the capacitance signal. The substitution of soda lime glass for doped silicon facilitated well-ordered capacitance signals and enabled increased relative change in capacitance

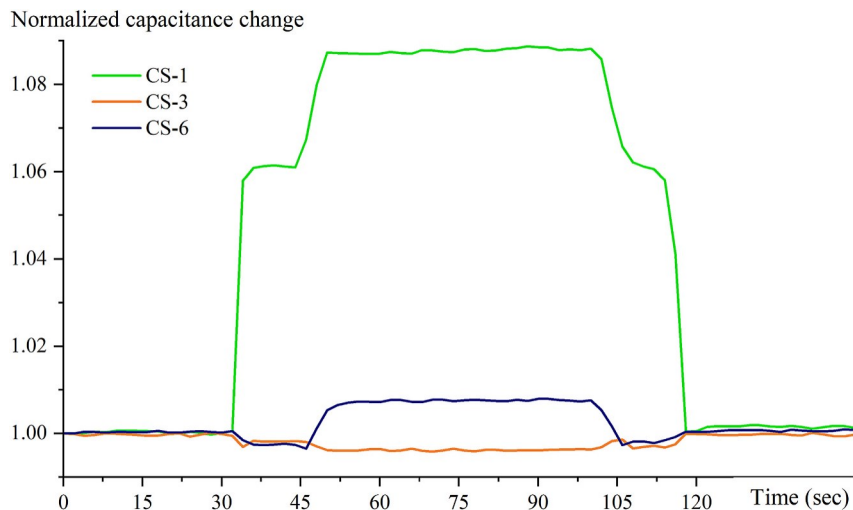


**Fig. 6.** Normalized capacitance changes with time for advancing and receding defionized water droplets using capacitance micro-sensors CS-1, CS-3, and CS-6 with the microdevice based on a doped silicon substrate.

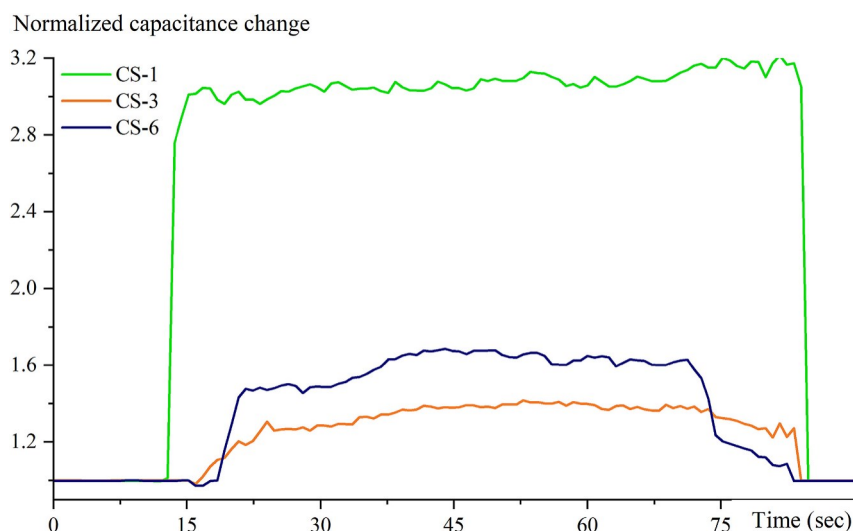


**Fig. 7.** Normalized capacitance changes with time for advancing and receding defionized water droplets using capacitance micro-sensors CS-1, CS-3, and CS-6 with the microdevice based on a soda-lime glass substrate.

compared to its semiconducting counterpart as shown in Fig. 7, where the same sensor combination from Fig. 6 (doped silicon) was used for capacitance sensing.

Based on results from the previous doped silicon substrate experiments [22], a sensor triplet comprising CS-1, CS-2, and CS-3 represents the most extreme scenario of sensor proximity effects where two out of three capacitance sensors exhibited inversion in their capacitance signals. Fig. 8 illustrates the relative change in capacitance for this sensor combination for doped silicon, where CS-1 still shows an uninterrupted detection of the spatial location of the MCL. The semiconducting base of the microdevice and the small spatial separation ( $\sim 40 \mu\text{m}$ ) among these immediately adjacent sensors are the major causes of this inversion, which constrained their simultaneous implementation in tracking MCL.

In comparison, adopting a dielectric base instead of the semiconducting one produced another improvement by weakening coupling effects, with only one sensor providing inverted signals shown in Fig. 9. As this data indicates, the experiment employed three sensors simultaneously in the highest sensor proximity configuration, where CS-3 contains inverted but still detectable MCL passage signals. Taken together, these experiments indicate the achievable limit of

spatial resolution ( $\sim 40 \mu\text{m}$ ) for this sensing scheme which essentially depends on the geometry and design of the sensor array regardless of the substrate material type.

During the above experiments, the DSA provided controlled dosing of the water droplet, where a short interval between successive dosing was maintained by pausing the droplet flow from the syringe to ensure a noticeable time lag among the sensors employed for tracking MCL. In contrast, during retraction, the suction of the water droplets through the syringe was uninterrupted and enabled a faster retraction motion of the MCL; consequently, retraction events happened faster than dosing events and thus demonstrated a smaller time lag. The experiments intended to allow a noticeable time lag among sensors to ensure individual functionality rather than an identical time lag for dosing and retraction.

To have more insights into the reason behind signal inversion when neighboring sensors are used requires scrutinizing Figs. 6–9 closely. Fig. 6 shows that the capacitance sensing based on a doped silicon substrate exhibited signal inversion of at least one sensor when three or more (out of six total) capacitance sensors were employed to track the MCL. According to the conceptual schematic of electrical field

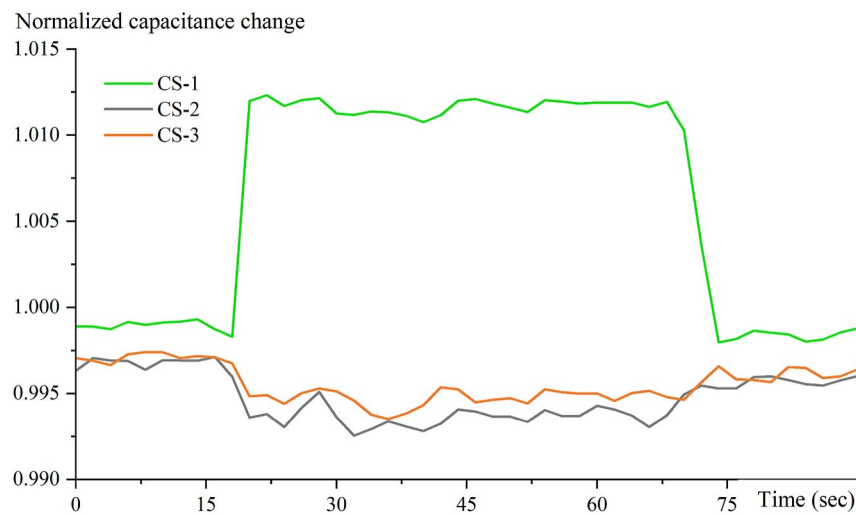


**Fig. 8.** Normalized capacitance changes with time for advancing and receding defionized water droplets using three capacitance micro-sensors (CS-1, CS-2, and CS-3) in adjacent proximity with the microdevice based on a doped silicon substrate.

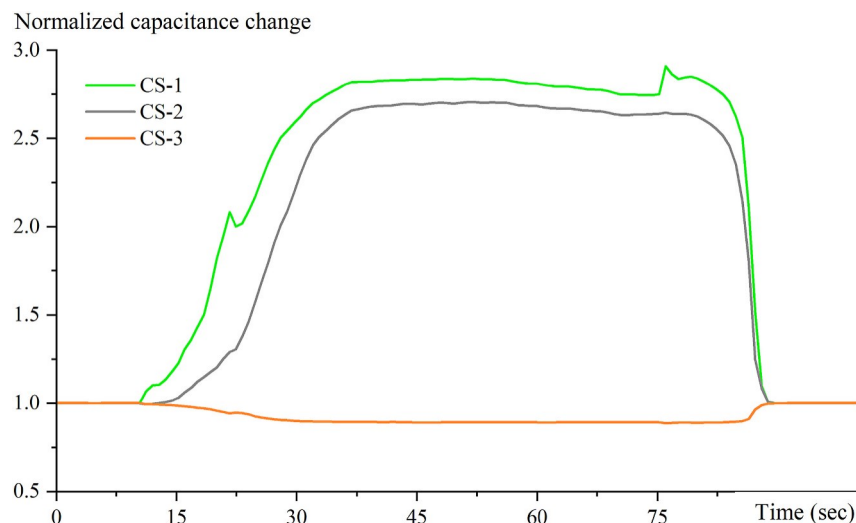


**Fig. 9.** Normalized capacitance changes with time for advancing and receding defionized water droplets using three capacitance micro-sensors (CS-1, CS-2, and CS-3) in adjacent proximity with the microdevice based on a soda-lime glass substrate.

distribution shown in Fig. 10, the electric field lines resulting from two adjacent IDE-based capacitance sensors interfere with each other. This interference or coupling effect among capacitance sensors placed adjacent to each other facilitates a variability in the electric field that drops the overall capacitance of the region. Therefore, electric field interference often led to signal inversion when neighboring sensors were used, especially for microdevices based on the doped silicon substrates. Later, an electrically insulating and lower dielectric constant substrate was adopted to overcome interference in capacititive signal outputs. Apart from lower dielectric constant, availability in conventional substrate form and cost-effectiveness made soda-lime glass an ideal candidate as the starting base of the microdevice. As shown in Fig. 7, the implementation of the soda-lime glass substrate abated the signal inversion caused by proximity effects.

Interestingly, another consequence of proximity effects was observed during the experiments, where the outermost sensor provided a signal with higher amplitude. To illustrate, CS-1 and CS-6, two external sensors in the sensing zone, enabled higher amplitude signals. These external sensors, surrounded by another sensor on a single side, experienced less interference or coupling than the interior sensors. In contrast, the

internal sensors, such as CS-3 (surrounded by other sensors on both sides), provided lower amplitudes due to interference from both sides.

The capacitance changes in the sensor array also enable location and speed tracking of MCL at elevated temperatures and in dynamic heat transfer processes such as occurs during the evaporation cycle of a water droplet. To investigate this, a thin-film resistance heater was integrated with the microdevice as described above, which facilitates heating of the topmost surface at various controllable temperatures. Figs. 11, 12, and 13 show the normalized change in the capacitance signal of six capacitance sensors during the evaporation cycle of a 1  $\mu$ L water droplet at surface temperatures of 57.2  $^{\circ}$ C, 70.7  $^{\circ}$ C, and 85.5  $^{\circ}$ C. These results indicate that, as expected, the duration of the evaporation event gets shorter as the surface temperature increases. According to the capacitance sensing perspective, the passage of the MCL due to the evaporation process occurred after 150 s at 57.2  $^{\circ}$ C, 106 s at 70.7  $^{\circ}$ C, and only 79 s when the surface temperature was at 85.5  $^{\circ}$ C. The DSA provided controlled dosing of the water droplet during experiments and captured images of the entire evaporation process during each of the experiments as shown in Fig. 4. During droplet evaporation studies, MCL's speed associated with the dosing was much lower than the speed of MCL due to

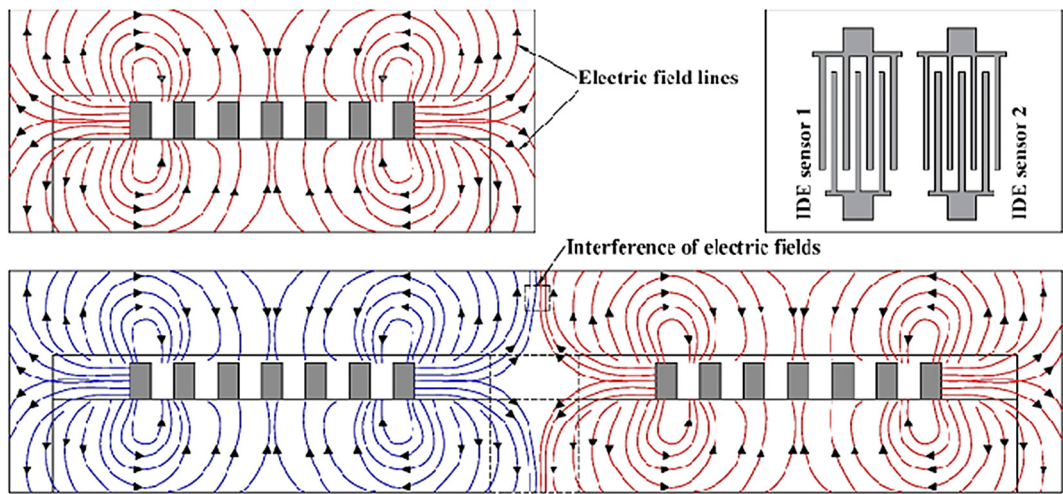


**Fig. 10.** Schematic of electric field lines distribution when a capacitance sensor is operating on its own (top) and when two IDE-based capacitance sensors are placed adjacent (bottom).

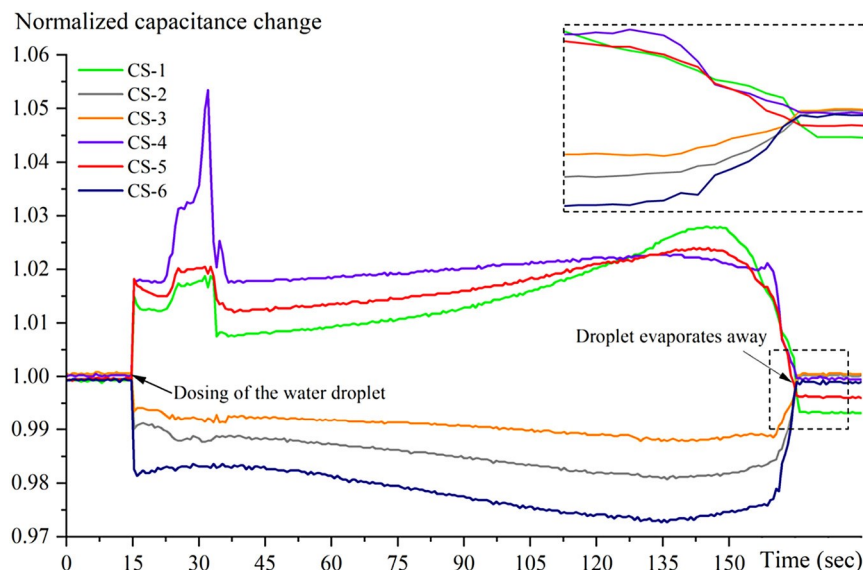


**Fig. 11.** Normalized capacitance changes with time for drop evaporation on a heated polyimide surface at 57.2 °C using six capacitance micro-sensors (CS-1 to CS-6). The dashed box on the top right shows a close-up of the time flag among the sensors as the drop evaporates away from the sensor region.

the evaporation at the near end of the experiment. Therefore, the MCL took a shorter time to move away from the sensor region, consequently demonstrating a shorter time lag during retraction.

The captured images of drop evaporation shown in Fig. 4 are in good qualitative agreement with the observed capacitance changes in the sensor array. As shown in Fig. 4, during the evaporation at 57.2 °C and 85.5 °C, the MCL of the water droplet moved away from the rightmost capacitance sensor (CS-6) to the leftmost one (CS-1). The normalized changes in capacitance signal shown in Figs. 11 and 13 exhibit the same sequence and time lag among each of the six sensors employed during the experiments. These results indicate the efficient functionality of this micro-device at elevated temperatures and during dynamic heat transfer processes.

Previous approaches within the literature to experimentally investigate the effects of drop evaporation under external electric fields have demonstrated very useful insights [28–30]. These works adopted parallel plate/disk capacitors to apply an external electric field to the droplet under study. High voltage power converters were employed to generate the high voltage between the capacitor plates such that the

applied electric fields were in kV/cm ranges. For noticing detectable changes in water droplet geometry such as contact angle, baseline, and surface area, the strength of the electric fields has to be quite strong, often in the several kV/cm range. In contrast, in our work each IDE-based capacitance sensor is connected to a function generator that provides a sinusoidal signal with a frequency of 200 kHz and amplitude of 7.07 Vrms. Even considering the microscale dimensions of our microdevice, we estimate a maximum possible field strength in the sensing region of less than 0.5 kV/cm, which is significantly smaller than field strength values in the literature [28–30]. Further, we have not observed any effects or changes in the geometry of the dosed water droplets during the experiments with the IDEs powered vs. not powered. For these reasons, we conclude that the applied voltage in our work was not strong enough to impose any impact on the droplet under study.

In the future, the improvement of this capacitance sensing micro-device should primarily focus on further reducing the proximity effect by enhanced filtering and minimizing parasitic capacitance in leads, traces, interconnects, other system elements. Another emphasis in device improvement should be increasing the spatial resolution, via more

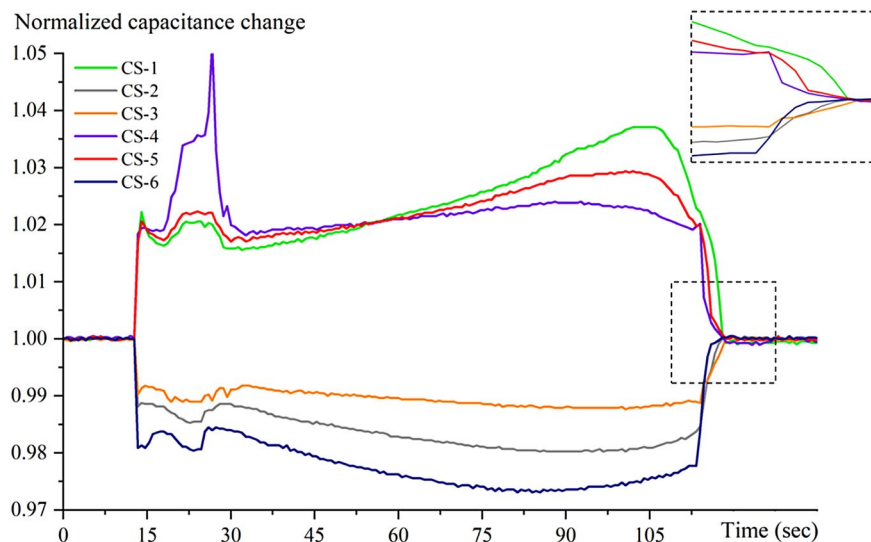


**Fig. 12.** Normalized capacitance changes with time for droplet evaporation on a heated polyimide surface at 70.7 °C using six capacitance micro-sensors (CS-1 to CS-6). The dashed box on the top right shows the time flag among the sensors as the droplet evaporates away from the sensor region.

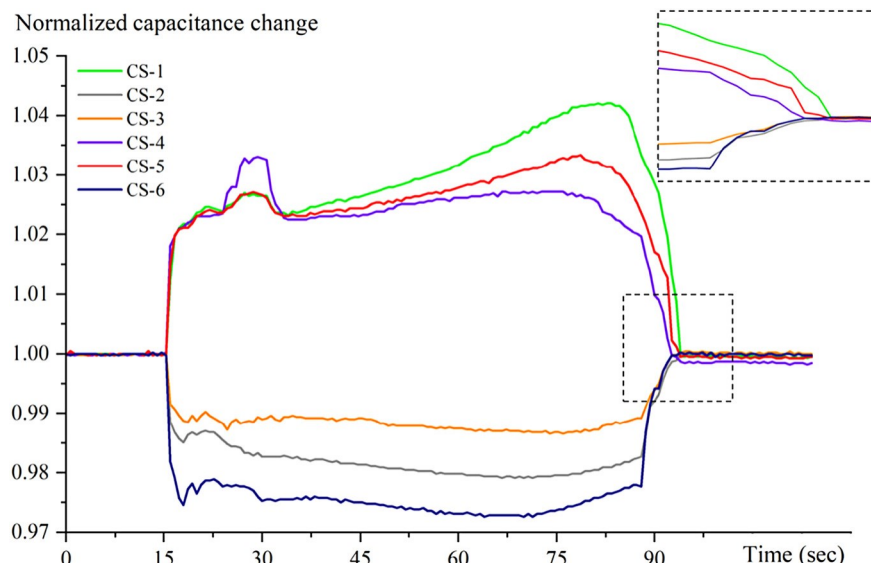


**Fig. 13.** Normalized capacitance changes with time for droplet evaporation on a heated polyimide surface at 85.5 °C using six capacitance micro-sensors (CS-1 to CS-6). The dashed box on the top right shows the time flag among the sensors as the droplet evaporates away from the sensor region.

compact geometry for the IDEs. This in turn, however, will require enhanced sensing of small capacitance changes and potentially more complicated micro/nanofabrication. For exploring new applications, this sensing scheme can be employed in complex phase-change heat transfer phenomena such as nucleate boiling processes and thin film evaporation. It may also be useful for application areas outside of thermal management such as water harvesting, pollutant detection, or immiscible liquid/liquid interface studies.

#### 4. Conclusions

In this work, we have presented a comparison of capacitive MCL tracking microdevice performance and its dependence on substrate type. The sensing scheme presented in this work has facilitated a highly sensitive and bulk-fabrication compatible means of MCL sensing, which is capable of tracking moving phase interfaces for unconstrained liquid droplets with both advancing and receding movement. Although the previous approach of implementing multiple capacitive sensors in

adjacent proximity for the semiconducting base has demonstrated a few limitations including coupling effects, it did not prevent the effective detection of MCL. Utilization of a dielectric substrate has demonstrated notable improvements, including but not limited to increased capacitance signal outputs and reduced coupling effects for multiple sensors in adjacent proximity. Moreover, this sensing scheme has demonstrated the efficient tracking of MCL during droplet evaporation at three different surface temperatures, which establishes its functionality at elevated temperatures and during a dynamic heat transfer process in the form of an evaporating water droplet. The future improvements related to this sensing scheme should emphasize increasing the spatial resolution and further reducing the proximity effect by minimizing parasitic capacitance.

#### Declaration of Competing Interest

The authors declare that there is no conflict of interest.

## Data availability

Data will be made available on request.

## Acknowledgements

This material is based upon work supported by the National Science Foundation under Grant Number 1846165.

## References

- [1] J. Eggers, H.A. Stone, Characteristic lengths at moving contact lines for a perfectly wetting fluid: the influence of speed on the dynamic contact angle, *J. Fluid Mech.* 505 (2004) 309–321.
- [2] A. Mohammad Karim, A review of physics of moving contact line dynamics models and its applications in interfacial science, *J. Appl. Phys.* 132 (8) (2022), 080701.
- [3] Y. Sufi, H. Ding, P.D.M. Spelt, Numerical simulations of flows with moving contact lines, *Annu. Rev. Fluid Mech.* 46 (2014) 97–119.
- [4] J.H. Snoeijer, B. Andreotti, Moving contact lines: scales, regimes, and dynamical transitions, *Annu. Rev. Fluid Mech.* 45 (2013) 269–292.
- [5] Y. Zhao, Moving contact line problem: advances and perspectives, *Theor. Appl. Mech. Lett.* 4 (3) (2014) 34002.
- [6] M.M. Nahar, et al., Review article: microscale evaporative cooling technologies for high heat flux microelectronics devices: background and recent advances, *Appl. Therm. Eng.* 194 (May) (2021).
- [7] S. Semenov, V.M. Starov, M.G. Vefarde, R.G. Rubrio, Droplets evaporation: problems and solutions, *Eur. Phys. J. Spec. Top.* 197 (1) (2011) 265–278.
- [8] R. Raj, C. Kunkele, P. Stephan, J. Pflawsky, J. Käim, Contact line behavior for a highly wetting fluid under superheated conditions, *Int. J. Heat Mass Transf.* 55 (9–10) (2012) 2664–2675.
- [9] K. Ibrahim, M.F. Abd Rabbo, T. Gambaryan-Rofisman, P. Stephan, Experimental investigation of evaporative heat transfer characteristics at the 3-phase contact line, *Exp. Thermal Fluid Sci.* 34 (8) (2010) 1036–1041.
- [10] M.J. Gibbons, P. Di Marco, A.J. Robinson, Local heat transfer to an evaporating superhydrophobic droplet, *Int. J. Heat Mass Transf.* 121 (2018) 641–652.
- [11] C. Kunkele, K. Ibrahim, N. Schweizer, S. Herbert, P. Stephan, T. Gambaryan-Rofisman, The effect of three-phase contact line speed on local evaporative heat transfer: experimental and numerical investigations, *Int. J. Heat Mass Transf.* 55 (7–8) (2012) 1896–1904.
- [12] H.K. Dhavalewarapu, S.V. Garimella, J.Y. Murthy, Microscale temperature measurements near the triple line of an evaporating thin liquid film, *J. Heat Transf.* 131 (6) (2009) 1–7.
- [13] J.L. Pflawsky, et al., Nano-and microstructures for thin-film evaporation—a review, *Nanoscale Microscale Thermophys. Eng.* 18 (3) (2014) 251–269.
- [14] P. Kubra Isgor, M. Marcali, M. Keser, C. Eflbuken, Microfluidic droplet content detection using integrated capacitive sensors, *Sensors Actuators B Chem.* 210 (2015) 669–675.
- [15] C. Eflbuken, T. Gflawdef, D. Chan, C.L. Ren, Detection of microdroplet size and speed using capacitive sensors, *Sensors Actuators A Phys.* 171 (2) (2011) 55–62.
- [16] E.V. Mofiseeva, A.A. Fletcher, C.K. Harnett, Thin-film electrode based droplet detection for microfluidic systems, *Sensors Actuators B Chem.* 155 (1) (2011) 408–414.
- [17] W. Wen Liu, Y. Zhu, 'Development and application of analytical detection techniques for droplet-based microfluidics—a review, *Anal. Chem. Acta* 1113 (2020) 66–84.
- [18] A. Ernst, W. Streul, N. Schmitt, R. Zengerle, P. Koifay, A capacitive sensor for non-contact nanofilter droplet detection, *Sensors Actuators A Phys.* 153 (1) (2009) 57–63.
- [19] M.C. Coyle, P.J.A. Kenis, Multiflexed electrical sensor arrays for microfluidic networks, *Sensors Actuators B Chem.* 136 (2) (2009) 350–358.
- [20] E.F. Crafton, W.Z. Black, Heat transfer and evaporation rates of small liquid droplets on heated horizontal surfaces, *Int. J. Heat Mass Transf.* 47 (6–7) (2004) 1187–1200.
- [21] S.A. Putnam, et al., Microdroplet evaporation on superheated surfaces, *Int. J. Heat Mass Transf.* 55 (21–22) (2012) 5793–5807.
- [22] M.T.H. Mondal, T. Desafi, R.E.-N. Hossain, A.L. Moore, Microscale tracking of unconstrained moving multiphase contact lines via a capacitance sensor array, *Sensors Actuators A Phys.* 331 (2021), 113046.
- [23] D. Nieto, T. Deigado, M.T. Flores-Arias, Fabrication of microchannels on soda-lime glass substrates with a Nd:YVO<sub>4</sub> laser, *Opt. Lasers Eng.* 63 (2014) 11–18.
- [24] H. Oi, et al., 6-inch uniform vertically-oriented Graphene on soda-lime glass for photothermal applications, *Nano Res.* 11 (6) (2018) 3106–3115.
- [25] C.H. Lin, G. Bfin Lee, Y.H. Lin, Y.H. Chang, A fast prototyping process for fabrication of microfluidic systems on soda-lime glass, *J. Microeng. Microeng.* 11 (6) (2001) 726–732.
- [26] J.Z. Chen, A.A. Darhuber, S.M. Troian, S. Wagner, Capacitive sensing of droplets for microfluidic devices based on thermocapillary actuation, *Lab Chip* 4 (5) (2004) 473–480.
- [27] C. Barbosa, C.A. Sifiva, T. Dong, Integratable capacitive bubble counter for lab-on-chip devices, in: 2014 IEEE International Symposium on Medical Measurements and Applications (MeMeA), 2014, pp. 1–5.
- [28] M.J. Gibbons, A.I. Garimella, S. O'Shaughnessy, P. Di Marco, A.J. Robinson, Evaporating hydrophilic and superhydrophobic droplets in electric fields, *Int. J. Heat Mass Transf.* 164 (2021).
- [29] P. Di Marco, R. Kurimoto, G. Saccone, K. Hayashi, A. Tomiyama, Bubble shape under the action of electric forces, *Exp. Thermal Fluid Sci.* 49 (2013) 160–168.
- [30] H. Alemohammadi, A. Amirkazemi, Sessile drop evaporation under an electric field, *Colloid Surf. A Physicochem. Eng. Asp.* 555 (2018) 580–585.